3D TOMOGRAPHIC RECONSTRUCTION FROM 2D DATA USING SPHERICAL HARMONICS

Louis M. Pecora
Code 6631
Naval Research Laboratory
Washington, DC 20375-5000

Abstract

Tomographic reconstruction of a 3D object in terms of spherical harmonics from a small number of 2D data sets is shown to be possible in cases of objects of high symmetry and/or low shape anisotropy. A test case using an object of cubic symmetry shows that the reconstruction can work well in such high symmetry cases when only two or three data directions are available. Numerical tests suggest that reconstructions are best done from data taken in low symmetry directions.

Introduction

In many fields the data obtained in "imaging" an object consists of a two dimensional (2D) array of points, each of which can be represented by an integral over some type of density associated with the object along a straight line through the object. The 2D arrays can be thought of as projections of the three dimensional (3D) density. In most cases what is desired is knowledge of the 3D density or object itself. The process of reconstructing the 3D density or object from the projections, usually called computer assisted tomography, is therefore, of great interest to many in these fields since it is generally the only way to get full 3D information about the object. In some fields such as electrom microscopy[1-6] and positron annihilation[7,8] the problem is made more difficult since it is often experimentally impossible to get more than a few projections of the object. Often, this difficulty is ameliorated by the existence of symmetry in the object, usually in the form of some point group consisting of rotations, inversions, and reflections.

This paper addresses the tomography problem under these latter conditions, although the technique presented here can be used in any tomographic situation. The density or object is represented by the scalar function $\rho(\bar{p})$ which maps the point $\bar{p} \in \mathbb{R}^3$ (the space of the object) to a value $\rho(\bar{p})$ in $\mathbb{R}^1$. In this paper, points in the space containing the object will be represented by $\bar{p}$'s and in the Fourier space will be represented by $\bar{r}$'s. The Fourier transform of the object $\rho(\bar{p})$ will be written as $\sigma(\bar{r})$. This notation is a derivative of that used in positron annihilation where $\rho(\bar{p})$ is the momentum density of the electrons in the object,[9] the measurements are made in momentum space $\bar{p}$ and the Fourier space is (by quantum mechanics) position space $(\bar{r})$. But the notation here is consistent in such a way that any 3D tomographic problem can be reformulated in terms of it.

The data must be represented as an integral over $\rho(\bar{p})$ along a line. It must remembered that the object will, in general, be rotated with respect to the laboratory frame of reference and this must be taken into account in the formulation of the problem. If R is the rotation matrix from the frame of the object to the lab frame and if $\bar{p} = (\xi, \eta, \zeta)$ is a point in the frame of the object then $R\bar{p} = (p_x, p_y, p_z)$ is the point in the lab frame. Similarly, the function $\rho(\bar{p})$ can be represented in the lab frame by using an operator $\underline{R}$ which transforms scalar functions from the object frame to the lab frame. Thus, in the lab frame $\underline{R}\rho$ is the function representing the density or object. Since $\rho(\bar{p})$ is a scalar function $\underline{R}\rho(R\bar{p}) = \rho(\bar{p})$. Now choose the rotation so that the line of integration representing the projection taking place in the experiment is along the z-axis in the lab frame. Then the equation for the data becomes

$$\left.\begin{array}{l}\text{data at point}\\ (p_x,p_y) \text{ with}\\ \text{rotation R}\end{array}\right\} = n^R(p_x,p_y) = \int_{-\infty}^{+\infty} dp_z \underline{R}\rho(R\bar{p}) \quad \text{(2D case)} \quad (1)$$

where the data $n^R(p_x,p_y)$ is labeled with R as the superscript to indicate, in a unique way, the orientation of the object when the data was taken. Another common case, given here for completeness, is that in which the measurement produces a projection which can be represented by a double integral over the object $\rho(\bar{p})$:

$$\left.\begin{array}{l}\text{data for the}\\ \text{point } p_z \text{ with}\\ \text{the rotation R}\end{array}\right\} = n^R(p_z) = \iint_{-\infty}^{+\infty} dp_x dp_y \underline{R}\rho(R\bar{p}) \quad \text{(1D case)} \quad (2)$$

where, here, R is the rotation which transforms the normal to the plane of integration in object frame to the z-axis in the lab frame. This is the familiar form of the 3D Radon transform.

There are several approaches to reconstructing objects from their integrals or projections.[10-12] One is to use back projection either in position space or fourier space. Another is to use purely numerical methods and reconstruct by some optimization procedure (often called algebraic reconstruction). A third method is to use an expansion of the object in known functions and solve for the coefficients in the expansion. I show below that the third method can be accomplished in 2D case (Eq. 1) using spherical harmonics and is feasible when the reconstructed object is known to have high symmetry and/or its anisotropies are small and "band limited" in angular variation, which are often the case in electron microscopy and positron annihilation.

The first reconstruction method using spherical harmonics was by P.E. Mijnarends[13] who solved the problem for the 1D case totally in momentum space. Later a Fourier or position space version of Mijnarends' method was developed by N.K. Hansen.[14] A somewhat different position space approach was also developed by Muller.[15] The first solution for the 2D case in momentum space was given by C.K. Majumdar,[16] who, in an elegant analysis, revealed many of the properties of the 2D case and first suggested that many terms in the spherical harmonic series could be obtained from only a few data projections. Another early solution for 2D case in terms of spherical harmonics was given by M.R. Howells and P.E. Osmon[17] who also presented their solution totally in momentum

space. Although Osmon and Howells took a somewhat different approach than Majumdar, they also came to the same conclusion that 2D data allows the determination of more terms in the series expansion than there are data projections available.

Other series expansion reconstruction techniques exist[16-18] which could be adapted to 3D reconstruction, but which would restrict the data directions to be in the same plane. Additionally, other reconstruction techniques have been applied to the positron 2D annihilation data.[19,20] The results have been quite good, but several directions (5 or more) are required to produce an adequately reconstructed $\rho(\bar{p})$.

The method in the present paper is the Fourier or position space version of Majumdar's 2D technique. As such it completes the set of available reconstruction techniques using spherical harmonics as shown in the table below:

Table 1

	1D case	2D case
Momentum space solution	Mijnarends (ref. 13)	Majumdar (ref. 16)
Position space solution	Hansen (ref. 14)	Present Work

In applying this technique to a model in this paper and to real data taken on a Vanadium single crystal,[21] I find that the conjecture by Majumdar and Osmon and Howells is correct: one can obtain more terms in the series expansion of spherical harmonics than there are data projections. This is not the case with the 1D projections. As will be seen below, the 2D case allows a very different treatment of the data.

Solution of the Problem

The solution of the 2D reconstruction problem in momentum space leads to exceedingly complex analytical equations[16,17] which make numerical evaluation difficult, if not intractable. This is probably why no reconstructions have yet been done using either Majumdar's[16] or Howells and Osmon's[17] methods. It turns out the solution of the problem in Fourier or position space is far simpler.

First, assume that $\rho(\bar{p})$ can be expanded in spherical harmonics[22]

$$\rho(\bar{p}) = \Sigma\, \rho_{\ell m}(p)\, Y_{\ell m}(\theta_p, \phi_p) \qquad (3)$$

where, $p=|\bar{p}|$ and $Y_{\ell m}$ are sherical harmonics. The exponential $e^{i\bar{p}\cdot\bar{r}}$ can also be expanded in spherical harmonics,

$$e^{i\bar{p}\cdot\bar{r}} = 4\pi\, \Sigma\, i^{\ell} j_{\ell}(pr) Y_{\ell m}(\theta,\phi)\, Y^{*}_{\ell m}(\theta_p,\phi_p) \qquad (4)$$

where θ_p and ϕ_p are the polar angles of the vector $\bar{p}$ and θ and ϕ are the polar angles of the vector $\bar{r}$. Then, it is easy to show that if $\sigma(\bar{r})$ is the Fourier transform of $\rho(\bar{p})$, it follows:

$$\sigma(\bar{r}) = \Sigma \sigma_{\ell m}(r)\; Y_{\ell m}(\theta,\phi) \qquad (5)$$

where, $r=|\bar{r}|$ and $\sigma_{\ell m}(r)$ and $\rho_{\ell m}(p)$ are related by the usual Hankel transform,

$$\rho_{\ell m}(p) = \frac{i^{\ell}}{2\pi^2} \int_0^{\infty} j_{\ell}(pr)\, \sigma_{\ell m}(r)\, r^2\, dr. \qquad (6)$$

Expression (6) allows one to use spherical harmonics as the basis in position space also and, therefore, do all the numerical work on the Fourier transforms of the data rather than on the data itself.

The problem now is to determine $\sigma_{\ell m}(r)$ from the data. This can be done by using the approach of Majumdar[16] as follows. Take the Fourier transform of the data,

$$\sigma^{R}(x,y) = \iint_{-\infty}^{\infty} dp_x dp_y\, n^{R}(p_x,p_y)\, e^{-i(p_x x+p_y y)}, \qquad (7)$$

here R also uniquely labels the Fourier transform.

By the Central Slice Theorem $\sigma^{R}(x,y)$ is equal to $\sigma(\bar{r})$ on a plane in position space which passes through the origin and is oriented such that its normal is just the ζ axis rotated by the rotation R. This is, of course, the z axis in the rotated system. So that from the various data projections information about $\sigma(\bar{r})$ is obtained on several planes in position space.

Now, as was the case for $\rho(\bar{p})$, $\sigma(\bar{r})$ can be written in the lab frame by using the rotation R and the associated function transformation $\underline{R}$. The Fourier transform in the lab frame is $\underline{R}\sigma$. The fact that σ is a scalar like ρ leads to the expansion of (r) in terms of spherical harmonics in the lab frame[22] which are represented by primed angle variables,

$$\sigma(\bar{r}) = \underline{R}\sigma(R\bar{r}) = \sum_{\ell mm'} \sigma_{\ell m}(r)\, D^{\ell}_{m'm}(R)\, Y_{\ell m'}(\theta',\phi') \qquad (8)$$

In Eq. (8) $D^{\ell}_{m'm}(R)$ are the expansion coefficients which depend on the Euler angles of the rotation[22-24] and $Y_{\ell m'}(\theta',\phi')$ are the spherical harmonics in the lab frame. Since the information $\sigma^{R}(x,y)$ is in the x-y plane, set z=0, i.e. $\theta'=90°$. Then write the spherical harmonics in terms of the associated Legendre polynomials and an exponential: $Y_{\ell m'}(\theta,\phi')= \overline{P}_{\ell m'}(0)e^{im'\phi'}$. Here I use the definitions of Altman and Bradley[23] for the spherical harmonics with $\overline{P}_{\ell m}$ being a normalized associated Legendre polynomial. With these substitutions Eq. (8) becomes

$$\sigma^{R}(x,y) = \sum_{\ell mm'} \sigma_{\ell m}(r)\, D^{\ell}_{m'm}(R)\, \overline{P}_{\ell m'}(0)\, e^{im'\phi'} \qquad (9)$$

All the quantities in Eq. (9), except, of course, $\sigma_{\ell m}(r)$, are known or can be calculated. This means Eq. (9) can be used as a linear system to solve for $\sigma_{\ell m}(r)$. However, it is better to do one more step which is quite natural because of the exponential nature of the right-hand-side of Eq. (9): take the polar Fourier transform of Eq. (9) with respect to ϕ'. Then

$$\sigma^{R}_{j}(r) \equiv \frac{1}{2\pi} \int_0^{2\pi} d\phi'\, e^{-ij\phi'} \sigma^{R}(x,y) = \sum_{\ell m} \sigma_{\ell m}(r)\, D^{\ell}_{jm}(R)\, \overline{P}_{\ell j}(0) \qquad (10)$$

where $r = (x^2+y^2)^{1/2}$ and $\phi' = \arctan(x/y)$. For the sake of clarity and later exposition let $H_{j,\ell m}(R) = D^{\ell}_{j'm}(R)\overline{P}_{\ell j}(0)$. Then Eq. (10) becomes

$$\sigma^R_j(r) = \sum_{\ell m} H_{j,\ell m}(R)\sigma_{\ell m}(r) \qquad (11)$$

The ϕ' polar transform is possible because of the 2D nature of the data (and therefore, it's Fourier transform). It is this feature which allows one to generate many independent equations in $\sigma_{\ell m}(r)$ for each rotation R. This allows for the solution of $\sigma_{\ell m}(r)$ to relatively high orders of ℓ. This is precisely the conjecture of Majumdar.[16] The only question left is the stability or well-posed nature of the system.[23] This system turns out to be quite stable when one "inverts" Eq. (11) using a least squares approach. The technical reason for this is given in Appendix 1. Here I write the equations for reference in the next section where the technique is applied. Remarks on the calculation of $D^{\ell}_{m'm}$, $\overline{P}_{\ell m}$, and $\overline{P}_{\ell m}(0)$ are given in Appendix 2.

Let $G=H^TH$, where H is the matrix in Eq. (11). Then, in more detail

$$G_{\ell m,\,\ell' m'} = \sum_{Rj} H_{j,\ell m}(R)\, H_{j,\ell' m'}(R). \qquad (12)$$

In symbolic form the solution is $(\sigma_{\ell m}(r)) = G^{-1}H^T(\sigma^R_j(r))$. Note that H and G are independent of r and only need to be calculated once in each reconstruction. After solving for $\sigma_{\ell m}(r)$ numerical integration using Eq. (6) will yield $\rho_{\ell m}(p)$.

In general the use of any reconstruction scheme employing spherical harmonics is limited by the assumption that the object to be reconstructed is "band" limited in angular variation. That is, there is some value of the spherical harmonic index, say ℓ_{max}, above which the $\rho_{\ell m}(p)$ are either zero or small enough not to affect the quality of the reconstruction. As will be seen in the next section, it is possible in many realistic situations to invert the matrix G for $\ell_{max} = 40$. For applications in solid state physics and, perhaps, other fields, this angular resolution will be superior to the resolution obtainable in the experiments which measure the projections n^R. At any rate, it is always possible with 2D data to test for the value of ℓ_{max} by calculating the polar Fourier coefficients of the data $n^R(p_x,p_y)$ and determining the highest frequency which is still above the noise level.[16]

A distinct advantage to the spherical harmonics approach is that it is straight-forward to take into account the point group symmetry of the object $\rho(\vec{p})$. The point group is the set (group, in the mathematical sense) of rotations, reflections, and inversions of the object about or through a point in the object space $(\vec{p})$ which leave the object unchanged. For example, an object with hexagonal symmetry is unchanged by rotations of 60° about the axis normal to the hexagonal symmetry plane. One can define new harmonics which are symmetrized linear combinations of the spherical harmonics.[25] Thus, the expansion of $\rho(\vec{p})$ becomes

$$\rho(\vec{p}) = \sum_k \rho_k(p)\, F_k(\theta_p,\phi_p) \qquad (13)$$

where $F_k(\theta_p,\phi_p) = \sum_{\ell m} A_{k,\ell m}\, Y_{\ell m}(\theta_p,\phi_p)$.

The coefficients $A_{k,\ell m}$ are chosen so as to keep F_k invariant under the operations of the symmetry point group (see Appendix 3 for more remarks on F_k). This eliminates any $Y_{\ell m}(\theta_p,\phi_p)$'s which do not have the proper symmetry. One then expands $\rho(\vec{p})$ up to some k_{max}. This often "compresses" the problem by reducing the dimension of the matrix G while retaining a large ℓ_{max} value. In terms of these new harmonics the appropriate equations are

$$\sigma^R_j(r) = \sum_k H_{j,k}(R)\,\sigma_k(r), \qquad (14)$$

with $H_{j,k}(R) = \sum_{\ell m} A_{k,\ell m} D^{\ell}_{m'm}(R)\overline{P}_{\ell j}(0)$, and

$$\rho_k(p) = \frac{i^{\ell}}{2\pi^2}\int_0^{\infty} j_{\ell}(pr)\,\sigma_k(r)\,r^2\,dr \qquad (15)$$

where ℓ depends on k. All the other equations for the solution follow in the same way.

Model Reconstruction

A model with cubic symmetry was chosen to test the 2D spherical harmonic reconstruction scheme. This consisted of a set of spheres with the following positions and weights or densities: a sphere of weight 1.0 centered at the center of a cube 18 units on a side, 6 spheres of weight 0.4 centered at 12 units from the cube center on either side of the origin along the (ξ,η,ζ) axes, and 8 spheres of weight 0.2 centered at the corners of the cube. The spheres are all 4 units in radius. The density is zero between the spheres. Figure 1 shows the model.

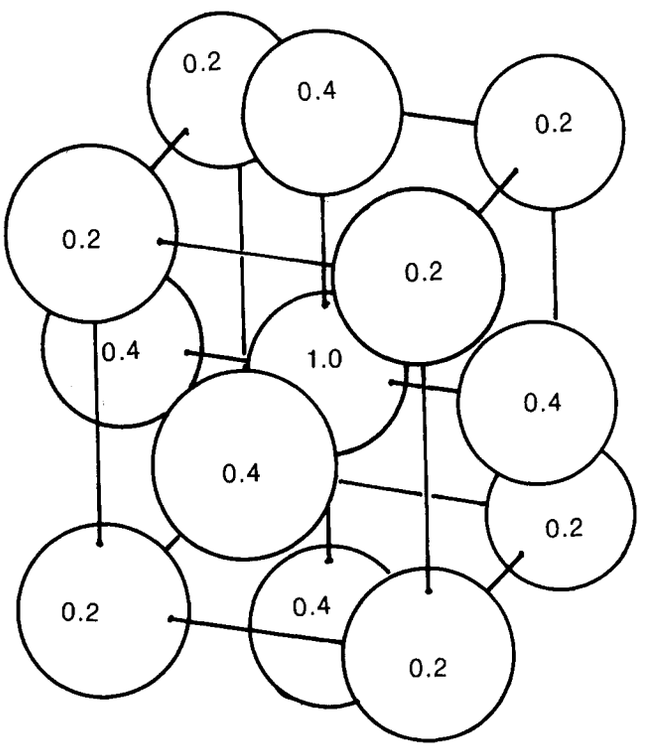

Fig. 1 Model used to test reconstruction scheme. Density of object is non-zero inside spheres (with weights as shown) and zero elsewhere.

Data was generated to produce two 2D projections: 1) z-axis (integration axis) oriented by the Euler angles $\alpha=30°$, $\beta=15°$, and$\gamma=0°$, and 2) z-axis oriented by $\alpha=10°$, $\beta=40°$, and $\gamma=0°$. The data arrays were from -24 units to +24 units in the x and y directions with grid or bin size equal to 0.25x0.25 units^2. This is equivalent to the type of data generated in a positron annihilation experiment. In the case of cubic symmetry the appropriate harmonics are cubic harmonics.[25] These were used to obtain the reconstruction of the model density employing the approach described above with a weight factor assigned as in Appendix I.

In this case it was found that truncation up to $k_{max}=40$ still lead to an invertible G matrix. However, because of the discontinuous nature of the density function of the model, the direct solutions tended to have wild oscillations near the boundaries of the spheres. In order to control this phenomena and to model a more realistic case, the solution was smoothed by multiplying the position (Fourier) space data arrays by a gaussian of FWHM=0.4 units. In this smoothed case, terms above k=25 made negligible contribution to the solution so that the solution presented here is nominally for $k_{max}=25$. This corresponds to $\ell_{max}=30$ or an angular resolution of $\sim 6°$.

The radial plots of the solution and the model are shown in Fig. 2. Surface plots of the solution and model are shown in Figs. 3, 4, and 5. The results can be seen to be quite good. Figure 6 shows a contour plot of Fig. 5. It shows that the outerlying spheres are well produced with little or no distortion in the shape of their surfaces.

Error Propagation

How does the propagation of errors look for each particular reconstruction? This, in principle, can be calculated directly since the reconstruction process is linear.

Let $B(\ell m,Rp_x p_y)$ represent the total operator used in the calculation of $\rho_{\ell m}(p)$ from data $n^R(p_x,p_y)$:

$$\rho_{\ell m}(p) = B(\ell m,Rp_x p_y) n^R(p_x,p_y), \tag{16}$$

where sums and integrals over the appropriate variables are implicit. Then the square of the standard deviation induced in the solution $\Delta\rho^2(\bar{p})$ by errors in the data represented by the square of the standard deviation of the data $(\Delta n^R(p_x,p_y)^2)$ is easily shown to be

$$\Delta\rho^2(\bar{p}) =$$

$$\sum_{\ell m}\sum_{\ell' m'} B(\ell m,Rp_x,p_y)\, B(\ell' m',\, Rp_x,p_y)\, Y_{\ell m}(\theta_p,\phi_p) \times$$

$$Y_{\ell' m'}(\theta_p,\phi_p)\, (\Delta n^R(p_x,p_y)^2), \tag{17}$$

The calculation of $B(\ell m,Rp_x,p_y)$ for the reconstruction is itself a formidable task. The calculations in Eq. (17) are thereby immensely difficult as they effectively involve the square of the operator and hence a large number of numerical operations.

Some preliminary results which involve using one gaussian to represent the error Δn^R in a positron annihilation experiment and examining only the $\ell=0$ terms of $\rho_{\ell m}(p)$ suggest that for the case of the model presented here and for the case of the application of this method to Vanadium data with 4 projections[14] the technique yields rather isotropic errors in the reconstruction which are of the order of a few percent when the data errors are of the order of 1%. The exception to this is near the origin where all reconstruction schemes have difficulty. There the error is of the order of 20%, but falls off rapidly to a few percent within 1 or 2 units radial distance from the origin.

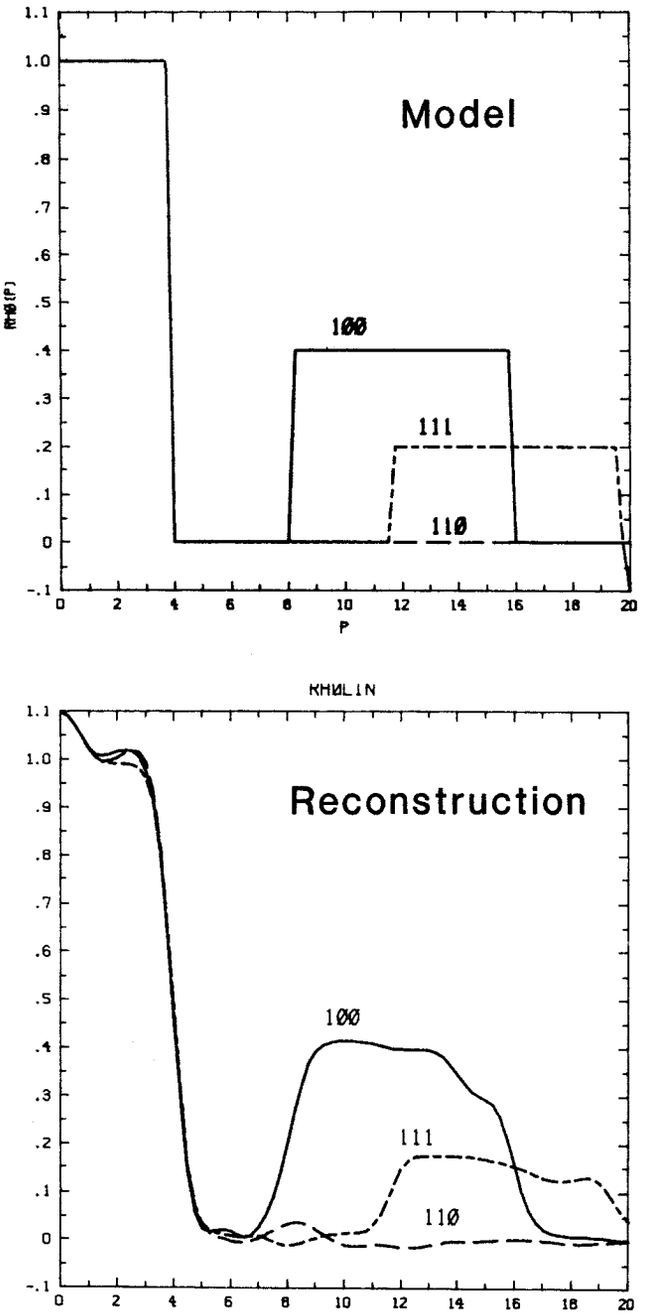

Fig. 2 Radial plots along cartesian axes (100), from origin to center of cube edge (110), and from origin to cube corner (111) of model and reconstruction of model from two projections.

Another approach to studying the propagation of errors which avoids the above analysis is a Monte Carlo method. That is, one generates errors in the data using a random number generator. The errors are distributed in a log-normal fashion at each point. The mean is taken to be zero and the standard deviation is the square-root of the number of counts in the the

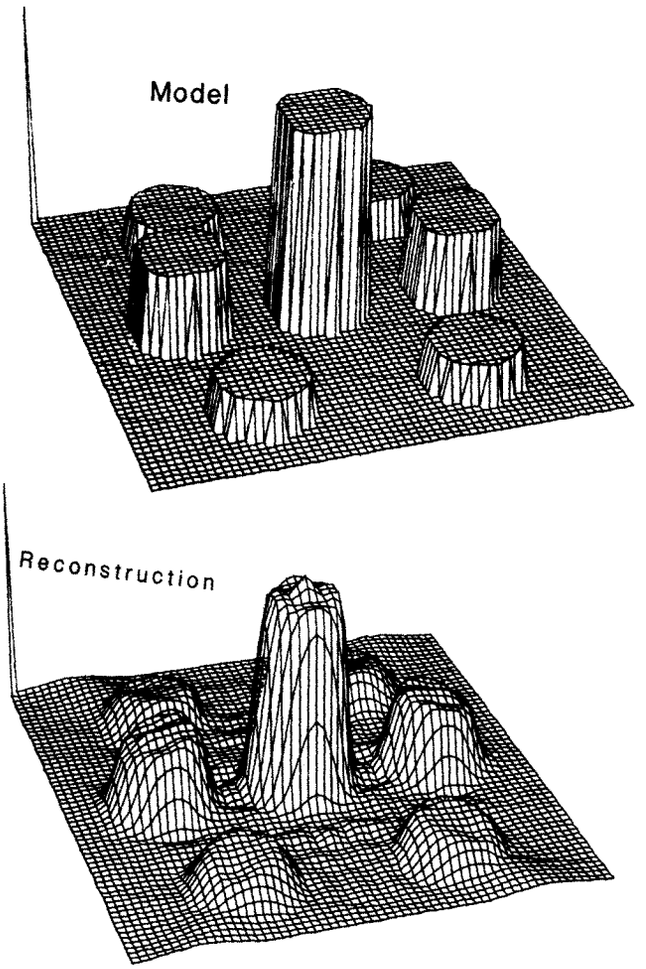

Fig. 3 Surface plot of model and reconstruction in an x-y plane.

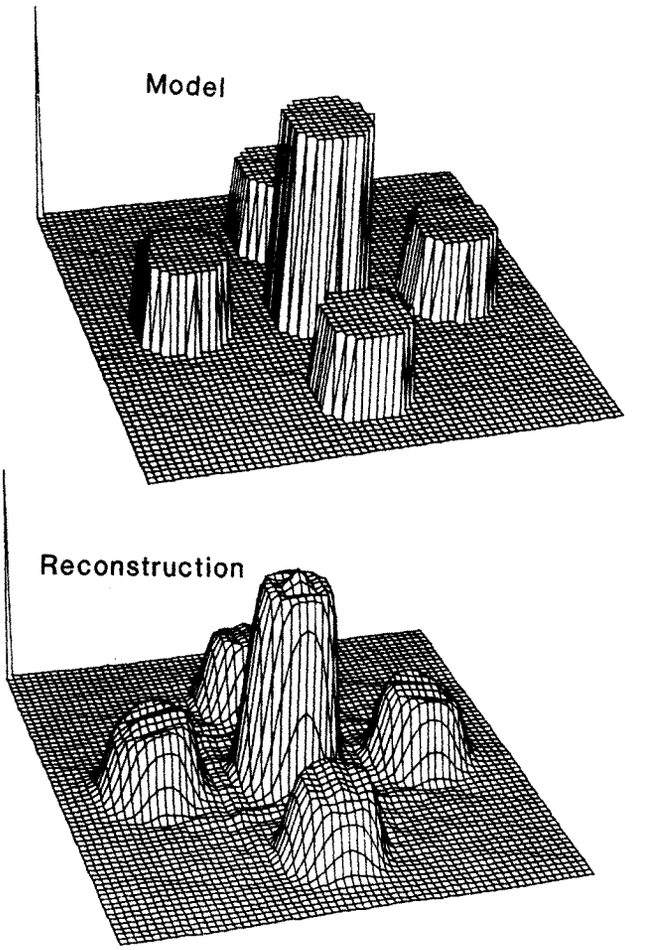

Fig. 4 Surface plot of model and reconstruction in an x-y plane rotated 45 degrees about the original y axis.

projection as in the usual statistics of image projections. Since the reconstruction operation is linear, one need only reconstruct an "object" from the error data arrays. Doing this for several different error data arrays a picture emerges of the expected error in the reconstruction.

This Monte Carlo procedure was done for the reconstruction of the Model in the previous section assuming 50,000 counts at the origin in the projections. It confirmed the preliminary results obtained in the direct analysis of error propagation: the errors were isotropically distributed in size and fell off rapidly in magnitude as a function of radial distance from the origin. Figure 7 shows an average of 4 Monte Carlo error reconstructions. The figure displays the standard deviation of the error in the reconstruction as a function of radial distance. The units are the same as Fig. 2 and allow a direct comparison. The angular isotropy of the reconstruction error presumably results from the high symmetry of the situation and the choice of the orientation of the data projections (see remarks in the Conclusions).

Conclusions and Remarks

The above model test and other tests done show that the reconstruction of 3D objects from 2D data can be accomplished using spherical harmonics and is especially applicable to cases of high symmetry and/or low object anisotropy. One particularly interesting finding was that the invertibility of the G matrix which is so crucial to the solution of the problem can be done for large ℓ_{max} values if the original 2D data is taken in planes of lowest symmetry rather than in high symmetry planes. This is apparent in the Table 2 below in which for a cubic system, the Euler angles of z-axis are given along with the largest k_{max} and ℓ_{max} value for which the G matrix can be inverted on a 32 bit computer using double precision arithmetic.

Table 2

Number of data sets	z-axis α	β		k_{max}	ℓ_{max}
1 (high symmetry)	0	0	0	1	0
1 (low symmetry)	71	33	0	10	16
2 (high symmetry)	0	0	0		
	0	45	0	5	10
2 (low symmetry)	71	33	0		
	54	43	0	30	32

Thus, in an experiment the data should be taken in planes of lowest symmetry. However, this is not typically the way positron annihilation data is taken (see Refs. 7 and 8). Although visual inspection of the 2D data is easiest in a high symmetry plane,

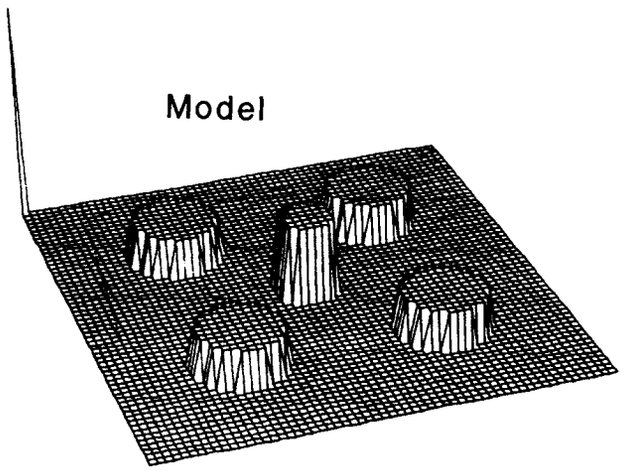

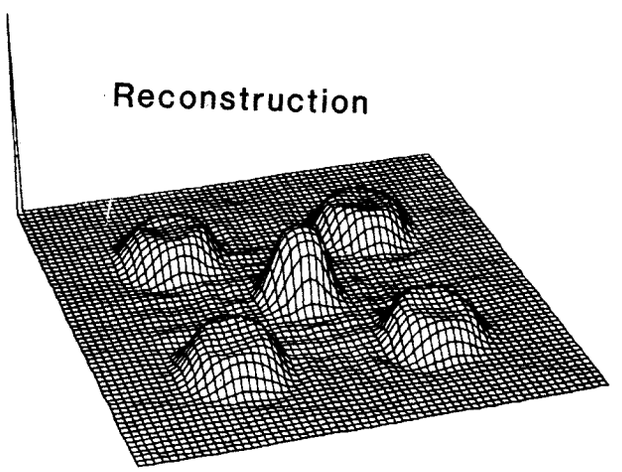

Fig. 5 Surface plot of model and reconstruction in a plane parallel to the x-y plane, but displaced by 6 units to coincide with the top of the cube in Figure 2.

if the experimenter is looking toward reconstruction, he will have to break with tradition to obtain the best results.

Table 2 implies that the stability of the inversion of the G matrix is highly dependent on the orientation of the projections n^R. However, the true calculation of the induced errors remains to be done.

Therefore, with judicious choices of projections, the technique remains a good option in situations with appropriate symmetry and in which a large number of data projections cannot be obtained.

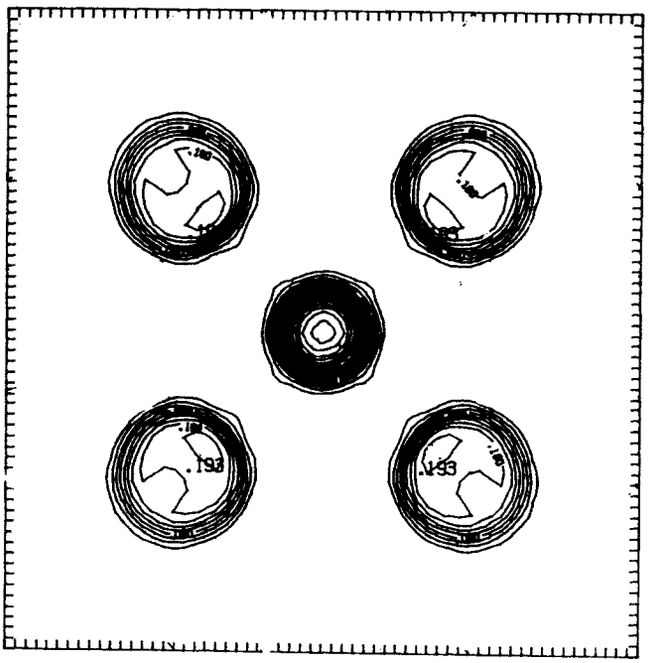

Fig. 6 A contour plot of Figure 5.

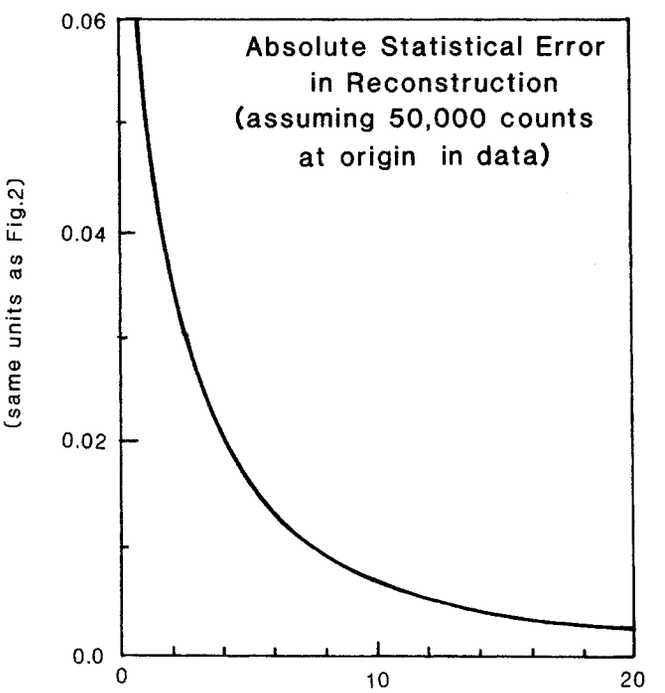

Fig. 7 The average statistical error in the reconstruction of the model from two projections using four sets of randomly generated error arrays. Ordinate units are the same as Figure 2.

Appendix 1

In the reconstruction of $\rho(\bar{p})$ it is necessary to invert the matrix $G=H^TH$. The reason this matrix can be inverted for large dimensions (30 - 40) is the following. G comes about because of a least squares solution to the linear equations in $\sigma(\bar{r})$. This least squares solution can be done with a weighting factor on each projection, i.e. for each R. The factor used here is the "natural" one of $\sin(\beta)\Delta\beta\Delta\alpha$, where α,β are the first two Euler angles and $\Delta\alpha$ and $\Delta\beta$ are rough measures of the average angles between projections, R. This gives for G

$$G_{\ell m,\,\ell' m'} = \sum_{jR} D^{\ell *}_{jm}(R)\, D^{\ell}_{jm'}(R)\, \bar{P}_{\ell j}(0)\bar{P}_{\ell' j}(0) \times \sin(\beta)\,\Delta\beta\,\Delta\alpha. \qquad (A1)$$

As the number of projections increases and they are roughly uniformly distributed over the unit sphere, the product of the $D^{\ell}_{m'm}(R)$ matrices and the solid angle $\sin(\beta)\,\Delta\beta\,\Delta\alpha$ approaches the integral $\int_0^{2\pi} d\alpha\, d\beta \sin(\beta)\, D^{*}_{jm'}((R)D_{jm}(R)$ which is equal to[22] $16\pi^3\delta_{m'm}\,\delta_{\ell'\ell}/(2\ell+1)$. G becomes nearly diagonal which helps to stabilize the inversion process. In the case of high symmetry objects the number of projections is effectively increased by the symmetry and they are generally spread evenly over the unit sphere. Therefore the method converges in the appropriate limit and is quite stable in many applications in which objects with high symmetry are being reconstructed.

Appendix 2

In the reconstruction using spherical harmonics it is often necessary to calculate quantities up to large ℓ values. This has also been noted by Heuser-Hofmann and Weyrich.[26] Here I give several recursion relations for doing this. These have been tested to at least ℓ=50 and appear to be quite stable. The quantities of interest are $\bar{P}_{\ell m}(\theta,\phi)$, $\bar{P}_{\ell m}(0)$, and $D^{\ell}_{m'm}(R)$.

A relatively stable recursion relation for the numerical calculation of (unnormalized) Legendre polynomials is[27] $P_{n+1}(x) = 2xP_n(x)-P_{n-1}(x)-[xP_n(x)-P_{n-1}(x)]/(n+1)$. This is easily generalized to (unnormalized) associated Legendre polynomials,

$$P_{\ell+1\,m}(x) = 2xP_{\ell m}(x)-P_{m-1}(x)-[(1-2m)xP_{\ell m}(x)+(2m-1)P_{\ell-1\,m}(x)]/(\ell-m+1). \qquad (A2\text{-}1)$$

To use normalized associated Legendre polynomials $\bar{P}_{\ell m}=N_{\ell m}P_{\ell m}$ where $N_{\ell m}$ is the normalization constant, simply substitute for $P_{\ell m}$ in Eq. (A2-1) to obtain

$$\bar{P}_{\ell+1\,m}(x)=2xR_{\ell m}(x)-S_{\ell m}\bar{P}_{\ell-1\,m}(x) - [(1-2m)xR_{\ell m}\bar{P}_{\ell m}(x)+(2m-1)S_{\ell m}\bar{P}_{\ell-1\,m}(x)]/(\ell-m+1) \qquad (A2\text{-}2)$$

where

$$R_{\ell m}=N_{\ell+1\,m}N^{-1}_{\ell m} = \left[\frac{(2\ell+3)}{(2\ell+1)}\cdot\frac{\ell-m+1}{\ell+m+1}\right]^{1/2} \qquad (A2\text{-}3)$$

$$S_{\ell m}=N_{\ell+1\,m}N^{-1}_{\ell-1\,m} = \left[\frac{(2\ell+3)}{(2\ell+1)}\cdot\frac{(\ell-m+1)(\ell-m)}{(\ell+m+1)(\ell+m)}\right]^{1/2}$$

It is simple to set up recurrence relations for $R_{\ell m}$ and $S_{\ell m}$. They need be calculated only once. The recurrence relation for the associated Ledendre polynomials is increasing in ℓ so that $R_{\ell m}$ and $S_{\ell m}$ approach 1 as the recurrence progresses. The recurrence appears to be quite stable. It has been tested using double precision arithmetic up to ℓ=100.

The calculation of $\bar{P}_{\ell m}(0)$ is done by utilizing the following formulas. $\bar{P}_{\ell m}(0)=0$ if $\ell-m$ is odd, otherwise $\bar{P}_{\ell m}(0)= [(2\ell+1)v_{\ell m}/2\pi]^{1/2}$ where $v_{\ell+1m+1}= (\ell+m+1)/v_{\ell m}/(\ell+m+2)$ and if m=0 divide by another factor of 2. The starting point for $v_{\ell m}$'s is $v_{00}=1$ and $v_{\ell+2\,0}= v_{\ell 0}(\ell+1)^2/(\ell+2)^2$.

The calculation of $D^{\ell}_{m'm}(R)$ can be done following the approach of Wigner[28] as outlined by Edwards[22] and Altman and Bradley.[23,24] Note that[23] $D^{\ell}_{m'm}(R)= e^{im'\gamma}d^{\ell}_{m'm}(\beta)e^{im\alpha}$. So that rotations about the z-axis only contribute exponential factors. Wigner's "trick" is to rotate to a new frame so that the y-axis rotation β is about the new z-axis. This is accomplished by a rotation of $\pi/2$ about z and a rotation of $\pi/2$ about the new y-axis. A rotation of β about the new z-axis then accomplishes the old y rotation. One, then returns to the old axes by a rotation of $-\pi/2$ about the newest y axis and a rotation of $-\pi/2$ about the new z-axis. This produces the equation[22]

$$d^{\ell}_{m'm}(\beta)= \sum_{m''\ell''} e^{im\pi/2}d^{\ell}_{m''m}(\pi/2)e^{im''\beta}d^{\ell}_{m'm''\ell''}(-\pi/2)e^{-im'\pi/2} \qquad (A2\text{-}4)$$

The problem now only remains to calculate $d^{\ell}_{m'\ell m}(\pi/2)$ as $d_{m'\ell m}(-\pi/2)$ is simply related to it.[23,24] Following Altman and Bradley[23,24] for fixed ℓ value and $\beta=\pi/2$ first calculate $d^{\ell}_{\ell\ell}=1/2^{\ell}$. Then obtain $d^{\ell}_{\ell m}$'s from $d^{\ell}_{\ell m-1}=d_{\ell m}[(\ell+m)/(\ell-m+1)]^{1/2}$. Finally, one does downward recursion on the other lower index using

$$d^{\ell}_{m'-1\ m} = \frac{(m'-m)}{\sqrt{(\ell-m+1)(\ell+m)}}\, d^{\ell}_{m'm} - \left[\frac{\ell+m}{(\ell-m'+1)(\ell-m+1)(\ell+m')}\right]^{1/2}(\ell+m+1)\, d^{\ell}_{m'\ m-1} \qquad (A2\text{-}5)$$

The programs to calculate these quantities have been checked against Altman and Bradley's tables of $d^{\ell}_{m'm}(\pi/2)$[23] up to ℓ=20, by checking the position of zeros in the arrays of values up to ℓ=50[23,24] and (most importantly) up to ℓ=50 by calculating $\sigma^{R}(r)$ values from chosen $\sigma_{\ell m}(r)$ values and then using G^{-1} to recover the $\sigma_{\ell m}(r)$'s.

Appendix 3

The subject of symmetrized combinations of spherical harmonics is a large one in itself and here I only intend to make a few remarks to introduce the reader to the idea. A mathematical development is given in Ref. 25.

If $\rho(\vec{p})$ is invariant under the operations of some point group (which are rotations, reflections, and/or inversions) it is more efficient to expand $\rho(\vec{p})$ only in those spherical harmonics or linear combinations of those which are also invariant under the operations of the group. This is the higher dimensional analog of, for example, using only cosine functions in a Fourier series expansion of an even function. In the text these symmetrized harmonics are written as F_k, where k merely enumerates the harmonics. For example, if an object $\rho(\vec{p})$ has hexagonal symmetry about some axis (taken as the z-axis here), then only those spherical harmonics $Y_{\ell m}$ for which m is a multiple of 6 can contribute to the expansion of $\rho(\vec{p})$. In addition, hexagonal symmetry implies invariance under reflections through planes which contain the symmetry axis and are 60° apart. There are 2 sets of these, with 6 in each set. This means that only even harmonics can contribute to the $\rho(\vec{p})$ expansion. This requires the (normalized) harmonics in the expansion of $\rho(\vec{p})$ to be the form $F_k = (Y_{\ell m} + Y^*_{\ell m})/2$, where $m = 6n$ $(n = 0, 1, 2, ..)$. So, by writing $\rho(\vec{p}) = \Sigma_k \rho_k(p) F_k(\theta,\phi)$ terms of the improper symmetry are eliminated at the outset and the dimension of the matrix to be inverted is correspondly reduced for fixed ℓ.

For objects with only one axis of n-fold symmetry (n>2) the above simple construction of F_k works well. For objects with more than one such axis the problem of finding F_k is more difficult and cannot be done in so straightforward a fashion. This latter case occurs, for example, in objects with tetrahedral, cubic, and icosahedral symmetry. For cubic symmetry a good reference which leads the reader through the elimination and combination of $Y_{\ell m}$ is Mueller, et al.[30] The associated cubic harmonics have been computed[31,32] up to ℓ=60. I have these in a computer file and will make them available to anyone needing them. Although icosahedral symmetry is common in certain electron microscopy applications,[1-6] I know of no calculation of the associated icosahedral harmonics for this case. Apparently this remains to be done.

References

1. R.A. Crowther, L.A. Amos, J.T. Finch, D.J. DeRosier, and A. Klug, Nature 226, 421 (1970).
2. R.A. Crowther, D.J. DeRosier, and A. Klug, Proc. Roy. Soc. Lond. A317, 319 (1970).
3. D.J. DeRosier, Contemp. Phys. 12, 437 (1971).
4. D.J. DeRosier and A. Klug. Nature 217, 130 (1968).
5. R.A. Crowther and P.K. Luther, Nature, 307, 569 (1984).
6. R.A. Crowther, Ultramicroscopy, 13, 295 (1984).
7. Positron Solid State Physics, ed by W. Brandt and A. Dupasquier (North Holland Publ. Co., New York 1983).
8. Positrons in Solids, ed. by P. Hautojarvi (Springer-Verlag, New York 1979).
9. More properly $\rho(\vec{p})$ is the two photon density (see Refs. 3 and 4) and represents the joint momentum density of the annihilating positron-electron pairs. However, for the sake of clarity, this point is ignored in this paper as it is irrelevant to the discussion.
10. G.T. Herman, Image Reconstruction from Projections: The Fundamentals of Computerized Tomography, (Academic Press, San Francisco, 1980).
11. R.S. McKay, Medical Images and Displays, (Wiley, NY, 1984).
12. The Radon Transform and Some of Its Applications, by S.R. Deans (John Wiley and Sons, New York, 1983).
13. P.E. Mijnarends, Phys. Rev. B160, 512 (1967).
14. N.K. Hansen, Rpt. No. B342, Hahn-Meitner-Institut, Berlin (1980).
15. F.M. Mueller, Phys. Rev. B15, 3039 (1977).
16. C.K. Majumdar, Phys. Rev. B4, 2111 (1971).
17. M.R. Howells and P.E. Osmon, J. Phys. F2, 277 (1972).
18. G. Kontrym-Sznajd, in Positron Annihilation, ed by P.G. Coleman, S.C. Sharma, and L.M. Dians (North Holland Publ. Co., New York, 1982).
19. R.L. Waspe and R.N. West, ibid.
20. F. Sinclair, W.S. Farmer, and S. Berko, ibid; S. Berko, in Positron Annihilation, Proc. of 5th Inter. Conf. on Positron Annihilation ed by R.R. Hasiquti, K. Fujawara (Japan Inst. Metals, 1979).
21. L.M. Pecora, A.C Ehrlich, A.A. Manuel, A.K. Singh, and R.M. Singru, in Proc. 7th Inter. Conf. on Positron Annihilation, ed by P.C. Jain, R.M. Singru, and K.P. Gopinathan (World Scientific, Singapore, 1985) p 254. 22. A.R. Edmonds, Angular Momentum in Quantum Mechanics, (Princeton Univ. Press, Princeton NJ, 1957).

22. A.R. Edmonds, Angular Momentum in Quantum Mechanics, (Princeton Univ. Press, Princeton NJ, 1957).

23. S.L. Altman, Proc. Cambr. Phil. Soc. 53, 343 (1957).

24. S.L. Altman and C.J. Bradley, Phil Trans. Roy. Soc. A255, 193 (1963).

25. S.L. Altman and A.P. Cracknell, Rev. Mod. Phys. 37, 19 (1965); S.L. Altman and C.J. Bradley, Rev. Mod. Phys. 37, 33 (1965).

26. E. Heuser-Hofmann and W. Weyrich, Z. Naturforsch. 40a, 99-111 (1985).

27. G. Arfken, Mathematical Methods for Physicists (Academic Press, New York 1970), chapter 12.

28. E.P. Wigner, "On matrices which reduce Kronecker products of representations of S.R. groups", 1951 (unpublished).

29. C.J. Bradley, Library of Congress, Washington, DC, USA (1961) collection No. 61-18944.

30. F.M. Mueller and M.G. Priestly, Phys. Rev. 148, 638 (1966).

31. K. Fox and B. Krohn, J. Computational Phys. 25, 386 (1977).

32. T. Kwiatkowski, S. Olszewshi, and A. Wierzbicki, Inter. J. Quan. Chem., 11, 21 (1977).